Pattern formation in 4:1 resonance of the periodically forced CO oxidation on Pt(110)

Prabha Kaira, Pablo S. Bodega, and Christian Punckt*
Fritz-Haber-Institut der Max-Planck-Gesellschaft, Faradayweg 4-6, 14195 Berlin, Germany

Harm Hinrich Rotermund†
Department of Physics and Atmospheric Science, Dalhousie University, Halifax, Nova Scotia, Canada B3H 3J5

Dagmar Krefting
Charité-Universitätsmedizin Berlin, Campus Benjamin Franklin (CBF), Hindenburgdamm 30, 12200 Berlin, Germany
(Received 11 January 2008; published 11 April 2008)

Periodically forced oscillatory reaction-diffusion systems may show complex spatiotemporal patterns. At high-frequency resonant forcing, multiple-phase patterns can be found. In the present work, the dynamics of turbulent CO oxidation on Pt(110), forced with the fourth harmonic of the system's natural frequency, is investigated. Experiments result in subharmonic entrainment, where the system locks to a quarter of the forcing frequency. Cluster patterns are observed, where different parts of the pattern show a defined phase difference. The experimental results are compared with numerical simulations using the realistic Krischer-Eiswirth-Ertl model for catalytic CO oxidation. Using the fourth harmonic of an uncoupled surface element's natural frequency, we find 3:1 entrainment with three-phase cluster patterns in a wide parameter range of forcing amplitudes and frequency detuning. Numerical analysis of the spatially extended, turbulent system reveals a remarkable upshift of the mean oscillation frequency compared to homogeneous oscillations. Using the fourth harmonic of the most prominent frequency found in the turbulent system results in four-phase patterns with partial or full 4:1 entrainment, depending on the forcing parameters chosen.

DOI: 10.1103/PhysRevE.77.046106 PACS number(s): 82.40.Ck, 82.40.Bj, 05.45.Xt, 05.45.Pq

I. INTRODUCTION

Nonlinear reaction-diffusion systems show a variety of spatiotemporal patterns ranging from pulse propagation, homogeneous oscillations, standing waves, and target patterns to spiral waves and chemical turbulence. In recent years, research in this area has focused on the manipulation and control of spatiotemporal dynamics. Both for the Belousov-Zhabotinsky (BZ) reaction and the catalytic CO oxidation on Pt(110), experimental methods are now available to change reaction kinetics globally and as well as locally [1–6]. Periodic forcing by varying one reaction parameter periodically has been shown to lead to qualitative changes of the system dynamics. Besides frequency-locked homogeneous oscillations, complex spatiotemporal phenomena may occur. Depending on the forcing frequency and amplitude, phase clusters, irregular and localized clusters, stripes, and labyrinthine patterns are observed [2,7,8]. Periodic forcing applied to a nonlinear oscillator can cause the system to become entrained to the forcing frequency and the system dynamics result to be periodic. This behavior, known as frequency locking, occurs over a wide range of forcing frequencies and amplitudes, commonly referred to as Arnol'd tongues. Entrainment—or frequency locking—to external periodic forcing can be observed in a wide range of biological, chemical, and physical systems: for example, in circadian rhythms [9] or in the tips of chemical spiral waves [10–12].

Theoretical work on resonantly forced oscillators has focused on the complex Ginzburg-Landau equation (CGLE), a generic equation for oscillatory systems close to the Hopf bifurcation, and some more system-specific reaction-diffusion models (FitzHugh-Nagumo and Brusselator model). Most studies are done in the nonturbulent regime. Results are available for 2:1, 3:1, and 4:1 forcing: Patterns consisting of alternating spatial domains with a phase shift of π are observed within the 2:1 resonance. At 3:1 forcing, three stable phase states give rise to three-phase patterns with spatial domains, phase-shifted by $2\pi/3$ [13]. 4:1 resonant forcing has shown to be more complex. Spatial domains may differ in phase either by π or $\pi/2$, depending on the forcing amplitude. At strong forcing, the stationary π fronts are stable and standing two-phase patterns prevail. As the forcing strength is decreased, stationary π fronts lose stability and split into pairs of propagating $\pi/2$ fronts [14].

Simulations in the turbulent regime are performed for resonant forcing of the CGLE in Benjamin-Fair instability [15,16] and the Krischer-Eiswirth-Ertl model (KEE) with 3:1 and 2:1 forcing [17]. Stationary clusters are found in 2:1 resonance for sufficiently high amplitude. Decreasing the amplitude, the separating border regions between the two phase states start to grow and become turbulent until the clusters become unstationary and the cluster pattern is replaced by turbulent patterns, a phenomenon known as "front explosion." For 3:1 forcing, similar behavior is found, but the phase fronts separating the three-phase clusters are moving. Furthermore, a bistable 2:1 entrained state with labyrinthine pattern is found in 3:1 forcing. To our knowledge, no simulations of 4:1 resonant forcing have been performed for oscillatory systems in a turbulent state.

Experimental studies on resonant pattern formation in oscillatory reaction-diffusion systems have been focused on the periodically forced light-sensitive BZ reaction, which is limited to stable, nonturbulent oscillations [18,19].

*Present address: Department of Chemical Engineering, Princeton University, Princeton, NJ 08544, USA.
†Corresponding author; harm.rotermund@dal.ca

The catalytic CO oxidation on Pt(110) single-crystal surfaces shows both stable oscillations as well as spiral-wave turbulence [20,21]: CO oxidation on Pt(110) proceeds via the Langmuir-Hinshelwood mechanism [22]; adsorption of CO and oxygen molecules on Pt(110) has to take place before carbon dioxide can be formed. The adsorption of oxygen is dissociative. The system is maintained far from thermodynamic equilibrium by a constant supply of fresh reactants and removal of the products in the ultrahigh vacuum (UHV) chamber. Interplay of the reaction, lateral diffusion of CO, and adsorbate-induced surface reconstruction give rise to rich spatiotemporal dynamics like homogeneous oscillations, target patterns, spiral waves, or chemical turbulence [23,24]. A parameter scan of entrainment states of the oscillating CO_2 production is available for forcing frequencies up to 2:1 resonant forcing [20]. Spatially resolved studies of the system being in a turbulent state are performed for presumed 1:1 [7], 2:1, and 3:1 resonant forcing [21]. In all cases, 2:1 entrained cluster patterns are observed, stationary in presumed 1:1 resonance, and slowly moving phase fronts at high-frequency forcing.

Due to technical limitations, the range of forcing parameters that can be experimentally realized is confined. High-frequency forcing with reasonable amplitudes is difficult to implement as the experimental setup is strongly damped. Recent developments now enable us to explore a wider range of forcing parameters, allowing us to reach frequencies of about 4 times the natural frequency of the oscillatory system [21]. In this paper we explore pattern formation of the forced CO oxidation on Pt(110) in the 4:1 resonance, both experimentally and numerically. The resulting patterns are analyzed using their phase and amplitude representations. The motion of cluster walls is determined by stroboscopic space-time plots. The obtained results are then compared and discussed in the last section.

II. METHODS

A. Experimental setup

Experiments are performed in an UHV chamber with a base pressure of 10^{-10} mbar. Photoemission electron microscopy (PEEM) is used to obtain spatially resolved images of adsorbate patterns on the catalytic Pt(110) surface [25]. Prior to the measurement, the Pt surface is prepared by repeated cycles of argon ion sputtering below $T=470$ K, oxygen treatment at $T=570$ K and $p_{O_2}=10^{-6}$ mbar, and subsequent annealing up to $T=900$ K. Periodic forcing is applied to the system by a periodic modulation of the carbon monoxide partial pressure $p_{CO}(t)$:

$$p_{CO}(t) = p_0(1 + a \sin \nu_f t), \tag{1}$$

where p_0 is the base pressure of CO, a is the forcing amplitude, and ν_f is the forcing frequency. As commercially available electronic solenoid valves show strong damping at high frequencies, the forcing is realized by a self-developed gas-regulating device. For detailed information, refer to [21].

TABLE I. Model parameters, where not noted otherwise.

k_1	3.14×10^5 s^{-1} mbar^{-1}	Impingement rate of CO
k_2	10.21 s^{-1}	CO desorption rate
k_3	283.8 s^{-1}	Reaction rate
k_4	5.86×10^5 s^{-1} mbar^{-1}	Impingement rate of O_2
k_5	1.610 s^{-1}	Phase transition rate
s_{CO}	1.0	CO sticking coefficient
$s_{O,1\times1}$	0.6	Oxygen sticking coefficient on the 1×1 phase
$s_{O,1\times2}$	0.4	Oxygen sticking coefficient on the 1×2 phase
$u_0, \delta u$	0.35,0.05	Parameters for the structural phase transition
D	40 μm^2 s^{-1}	CO diffusion coefficient
p_{O_2}	12.0×10^{-5} mbar	O_2 partial pressure
p_O	4.6219548×10^{-5} mbar	Base CO partial pressure

B. Numerical model

The KEE model [26] takes adsorption of CO and oxygen molecules, reaction rates, desorption of CO molecules, the structural phase transition of the Pt(110) surface, and surface diffusion of adsorbed CO molecules into account. Surface faceting, formation of subsurface oxygen, and the effects of internal gas-phase coupling are not considered. The state of the system is determined by $u(\mathbf{r},t)$, $v(\mathbf{r},t)$, and $w(\mathbf{r},t)$, describing the surface coverage of CO, O, and the fraction of the nonreconstructed 1×1 surface, respectively. The time evolution of these fields is given by

$$u_t = k_1 s_{CO} p_{CO}(1-u^3) - k_2 u - k_3 uv + D\nabla^2 u,$$

$$v_t = k_4 p_{O_2}[s_{0,1\times1} w + s_{0,1\times2}(1-w)](1-v)^2 - k_3 uv,$$

$$w_t = k_5\left(\frac{1}{1+\exp[(u_0-u)/\delta u]} - w\right). \tag{2}$$

Numerical simulations are performed using a second-order finite-difference scheme for the spatial discretization with a grid resolution of $dx=4$ μm. For integration, an explicit Euler scheme with a fixed time step $dt=0.001$ s is used. The system size is 400×400 μm^2, and no-flux boundary conditions are applied. Periodic forcing is applied to the system according to Eq. (1). In the present study, the initial values for the partial pressures are chosen such that the unforced system oscillates and spontaneously exhibits spiral-wave turbulence. Model parameters are given in Table I. For a detailed description, refer to [17].

C. Pattern analysis

For further analysis, either the experimentally obtained PEEM image sequence or (for model simulations) the numerical values of the CO surface coverage are used. The course of time is visualized by space-time plots, showing the pattern evolution along a chosen line within the two-

dimensional data as a function of time. Oscillatory behavior as well as motion of cluster boundaries cross-sectioning this line can be determined from these plots. Furthermore, the average image intensity in a small region of the platinum surface is shown in comparison to the forcing as a function of time. From these plots, the state of entrainment can be easily determined. To measure the temporal response of the pattern, a frequency demodulation technique is used. At each image pixel the brightness of the image is recorded, giving us an ensemble of time series of the local system dynamics. The Fourier transform of these time series is calculated, and the complex Fourier coefficients of the main frequency component allow for amplitude and phase representations of the data. The spatial distribution of amplitude and phase is analyzed as well as the overall distribution of phase states, given as phase histogram and mapping into the complex plane.

III. RESULTS

A. Experimental results

The initial parameters for the experiment are chosen in such a way that the unforced system exhibits spiral-wave turbulence. The natural frequency of the system is defined by the maximum line of the Fourier spectrum of a 100-μm^2 surface region (for further details, see [21]). Applying 4:1 resonance forcing, we observe four-phase patterns.

At a forcing amplitude of $a=0.068$, the spiral-wave turbulence develops into stripelike wave fronts that periodically appear on the platinum surface [see Figs. 1(a) and 1(b)]. Figure 1(c), which gives the time course of the surface marked by the square in the first image of Fig. 1(a) (solid line) and the course of the forcing signal (dotted line), shows the subharmonic entrainment of the system to the forcing frequency. During four cycles of the forcing signal, the system performs one cycle of periodically changing from low to high CO coverage, indicated by low and high PEEM intensity, respectively. While small changes within the PEEM signal occur at all phases of the forcing frequency, the sudden increase of the CO coverage is in phase with the rising edge of the applied CO pressure. The same could be observed for the strong decrease of the CO coverage occurring in accordance with every fourth trailing edge of the forcing signal. The moment of high and low CO coverage occurs at different phases of the subharmonic oscillation for different places on the surface. It can best be seen in the space-time plot,

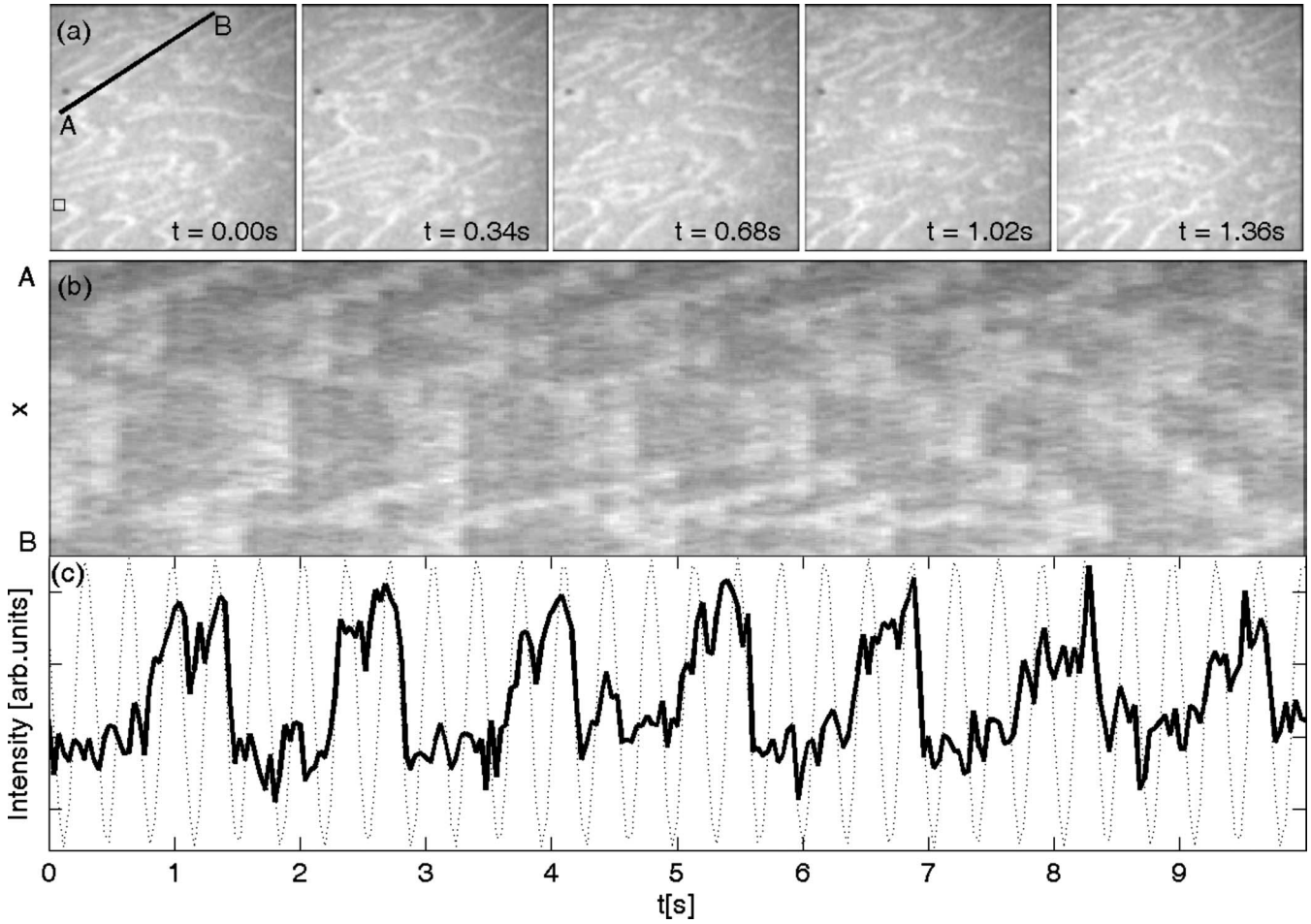

FIG. 1. Four-phase cluster formation and entrainment at 4:1 resonant forcing. (a) Snapshots of PEEM images (size 300×300 μm^2). (b) Space-time plots showing the pattern evolution along the AB line indicated in (a). (c) Averaged intensity of a local area of the surface (solid line), indicated by the square in (a), and the forcing signal (dotted line). Scaling is chosen to show both signals overlaid. The reaction parameters are $T=543$ K, $p_{O_2}=1.7\times10^{-4}$ mbar, $p_0=5.88\times10^{-5}$ mbar, $\nu_0=0.72$ Hz, $\nu_f=2.88$ Hz, and $a=0.068$.

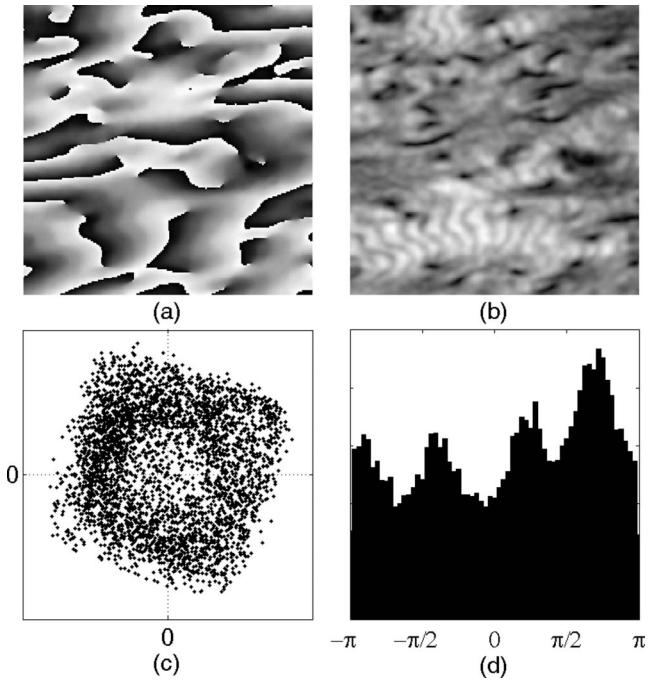

FIG. 2. Phase and amplitude representations of the cluster patterns shown in Fig. 1. (a) Phase pattern, (b) amplitude pattern, (c) phase portrait, and (d) phase histogram.

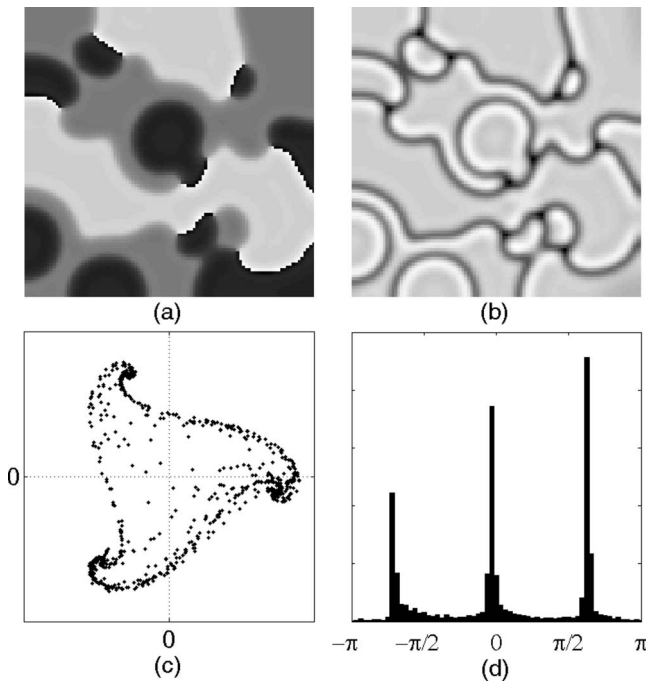

FIG. 3. Phase and amplitude representations of the cluster pattern, using the KEE model with forcing parameters $\nu_f=1.567$ Hz and $a=0.065$. (a) Phase pattern, (b) amplitude pattern, (c) phase portrait, and (d) phase histogram.

given in Fig. 1(b). It shows the intensity along the line indicated in the first image of Fig. 1(a).

Spatially resolved analysis of the appearing pattern using the demodulation technique shows phase clusters; see Fig. 2(a). Along with a notable amount of phase defects, indicating that the system is still turbulent, especially in the upper right area and the lower part of the analyzed surface, a regular four-phase pattern can be observed. The different phase states are visible in the phase pattern in Fig. 2(a) as black, dark-gray, gray, and light-gray areas. These areas show also a higher oscillation amplitude, given as bright areas in Fig. 2(b), while the domain interfaces are visible as regions with reduced amplitude, given in gray. The regions with strongly reduced amplitude near zero, seen in black, are located at the defect points. The two areas of high amplitude and regular phase pattern are separated by a turbulent regime, where the number of defects is larger and phase clusters cannot be identified. The phase portrait and the phase histogram, given in Figs. 2(c) and 2(d), show the presence of four distinct phase states with a phase difference of $\pi/2$, accompanied by an underlying random phase distribution due to the turbulent regime.

B. Numerical results

First attempts follow Ref. [17], where the system is forced with the nth harmonic of the oscillation frequency ν_0, obtained by the single-oscillator model ($\nu_{0,single}$). Using the same model parameters for the KEE model as [17] (see Table I), we applied the fourth harmonic of the generic frequency $\nu_f=4\nu_{0,single}$. Even if sometimes transient 4:1 entrainment was observed, long-term simulations always ended up in 3:1 entrainment and three-phase patterns or—at high amplitude—in homogeneous oscillations with 1:1 entrainment to the forcing frequency.

The phase and amplitude representations of a typical result are given in Fig. 3 for $a=0.065$. The three different phase states can clearly be seen in the phase plot (a) and the phase portrait (c). All phase states appear with the same amplitude (b), the phase fronts show decreased amplitude, and amplitude defects—i.e., points where the amplitude is decreased to zero and the phase is undefined—appear at locations where all three phase states meet. The histogram (d) shows that the phase states differ in $2\pi/3$.

A possible bistability between 3:1 and 4:1 locking, similar to the bistability of 3:1 and 2:1 near $\nu_f=3\nu_0$ found by Davidsen *et al.* [17], could not be verified. We could not find a 4:1 regime within the vicinity of the $\nu_f=4\nu_0$. Therefore we performed a frequency analysis of the simulated unforced extended system, which is in close relationship to the procedure of determining the natural frequency in the experiments.

To get an overview over the oscillatory characteristics of the extended system, we performed Fourier analysis of the free-running system in a fully developed turbulent state, using a time window of 81 s. Figure 4(a) shows the most prominent frequency $\nu_{\max}$ for each surface element. The local generic frequency variation spans a frequency range from 0.4 to 0.6 Hz. A certain frequency range is expected because of the turbulent state, but the distribution of measured local oscillation frequencies, shown as a histogram in Fig. 4(b), indicates that the mean frequency of 0.51 Hz is remarkably higher than the oscillation frequency of the single oscillator, which is rarely found in the extended system.

Figure 5 shows the course of both characteristic frequencies, the mean frequency of the extended system (squares)

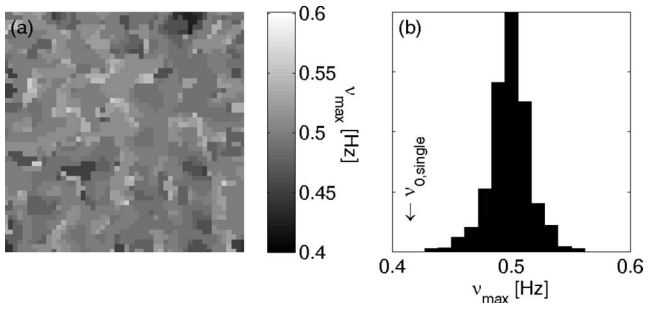

FIG. 4. Spatial distribution (a) and histogram (b) of the most prominent frequency $\nu_{\max}$ of the unforced KEE model in the turbulent regime. $\nu_{0,single}$ denotes the natural frequency of a single oscillator using the same reaction parameters.

and the natural frequency of the single-oscillator model, with increasing CO base pressure p_0. At the borders of the turbulent regime, homogeneous oscillations are found in the extended system, where the system behaves as a single oscillator. A maximum frequency difference of more than 0.1 Hz appears in the center of the turbulent regime, at $p_0=4.63\times10^{-5}$ mbar.

Defining the characteristic frequency of the extended system, $\nu_{0,\text{ext}}$, as the mean local oscillation frequency, we obtain for the chosen parameter set $\nu_{0,\text{ext}}=0.51$ Hz$\approx1.2\nu_{0,single}$. Therefore $\nu_f=4\nu_{0,single}$ corresponds to $\nu_f=3.3\nu_{0,\text{ext}}$. With respect to the natural frequency of the extended system, the forcing can be seen as a mismatched 3:1 resonant forcing rather than 4:1 resonant forcing. These findings explain the 3:1 entrainment when forcing with the fourth harmonic of the single oscillator's natural frequency and the absence of 4:1 entrainment.

Applying a forcing frequency of $\nu_f=2.04$ Hz, at $a=0.086$ the system is entrained and four-phase clusters appear. Snapshots of the pattern, the evolution along a line

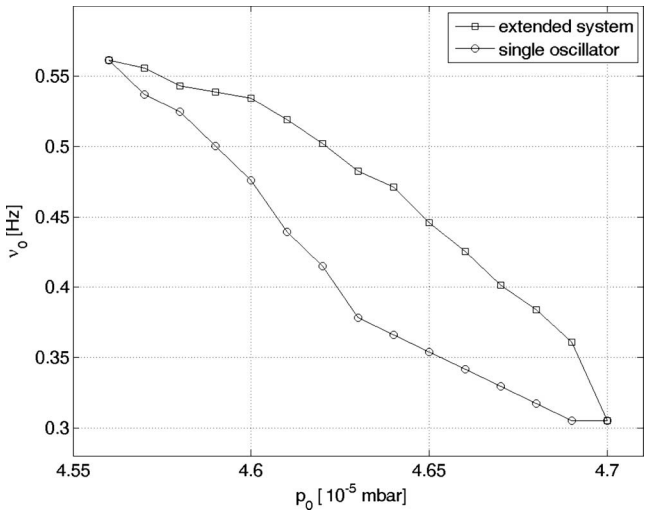

FIG. 5. Oscillation frequency of a single oscillator (circles) and mean oscillation frequency of the extended system (squares) using the KEE model with different p_0 within the turbulent regime. The end points, where both frequencies coincide, indicate the onset of homogeneous oscillations.

section, and the CO coverage for a sample point are presented in Fig. 6. Phase and amplitude representations are given in Fig. 7. The snapshots show separated phase clusters, which repeat every four cycles of the forcing period. The boundaries of the phase clusters seem to move from one forcing cycle to the other. This is visible in the space-time plot, where the bright clusters seem to shrink, but then recover to their original width within the next cycle of the system's oscillation [covering four cycles of the forcing signal, as can be seen in Fig. 6(c)]. The phase representation again shows the prominence of four-phase states, visible as four different gray levels in Fig. 7(a) and as highly populated points in the phase portrait (c). The histogram (d) shows the high density of four different phase states, where the maxima have a phase difference of $\pi/2$. The phase fronts between the clusters are represented by lines of low amplitude in Fig. 7(b). Most phase fronts are $\pi/2$ fronts. Where π fronts appear, the boundaries are broadened. At locations where more than two phase clusters meet, amplitude defects are present. The phase fronts are not stationary, but move slowly and may disappear, while others are created. Figure 8 shows a stroboscopic space time plot, where the CO coverage u is shown along a vertical line of the surface every fourth forcing cycle. The movement of the cluster boundaries is clearly visible. The phase-front velocity varies. This might be due to varying orientation of the phase front's normal to the intersection as well as due to different curvature of the phase front. Increasing the amplitude, moving four-phase clusters are observed until the system changes to 1:1 entrainment with homogeneous oscillations.

As due to local analysis and finite-frequency resolution of 0.02 Hz within the experiments, the estimation of the natural frequency is subjected to errors, which may result in a slight frequency mismatching. Therefore we simulated the response of the system under moderate detuning. The system is driven with $\nu_f=2$ Hz, keeping the amplitude at $a=0.086$.

Results are presented in the time domain (Fig. 9) as well as in the Fourier domain (Fig. 10). The snapshots of the CO coverage, given in Fig. 9(a), partially show turbulent behavior. Few-phase clusters with locally homogeneous CO coverage are visible, mainly located at the borders of the surface. Large parts of the surface show no sharp phase fronts, but a smooth change of u. They exhibit quasiperiodic behavior, as deviations from periodic behavior are not visible on small time scales of a few forcing periods T_f. Although the space-time plot and the local time series show no qualitative difference from the system at resonant forcing (compare to Fig. 6), analysis of the phase and amplitude representations, given in Figs. 10(a) and 10(b), reveals an increased number of topological defects. Large parts of the system feature a decreased oscillation amplitude while the phase clusters appear as regions with high amplitude, visible as bright regions in Fig. 10(b). It can also be seen in the phase portrait, given in Fig. 10(c), that the phase-amplitude distribution of the surface elements is less concentrated at maximum amplitude. The phase histogram, presented in Fig. 10(d), still contains four peaks with phase difference of $\pi/2$. In comparison to resonant forcing [see Fig. 7(d)], the fraction of elements with random phase is increased, similar to the experimental result. As these characteristics are maintained even for long-term

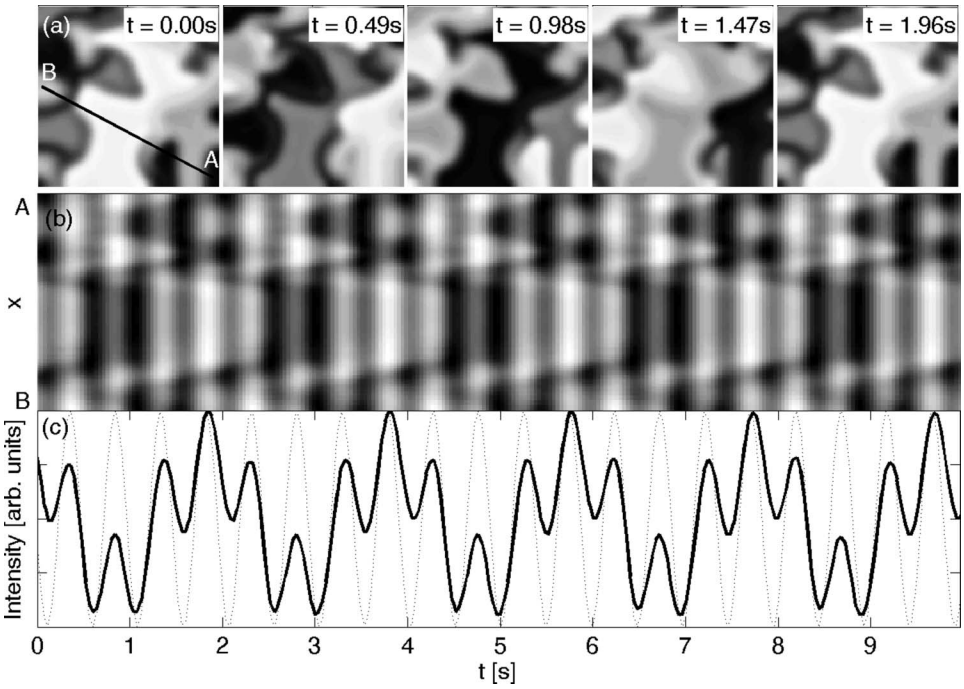

FIG. 6. Four-phase cluster and entrainment at 4:1 resonant forcing, KEE model. (a) Snapshots of CO coverage (size $400 \times 400\ \mu m^2$). (b) Space-time plot along the *AB* line (see top panel). (c) Local CO coverage at point *A* and forcing signal (dotted line). Model parameters: $\nu_f = 2.04$ Hz and $a = 0.086$.

simulations ($t > 400T_f$), we assume an asymptotic state rather than transient behavior.

IV. CONCLUSION

We have investigated pattern formation in turbulent CO oxidation on Pt(110), forced by an external homogeneous periodic perturbation. The scenario of 4:1 resonant periodic forcing of the CO catalysis on Pt(110) has been characterized in detail using both experimental and theoretical approaches.

Experimentally, 4:1 entrainment and four-phase cluster patterns could be observed. However, the cluster formation takes place in finite regions of the surface, while other parts appear not to be 4:1 entrained, but still show turbulent behavior. This is one of the reasons why global coupling [26,27] can be neglected in our study. Global coupling can stabilize homogeneous oscillations in a large surface area. Our system, however, breaks up into a large number of rather small clusters. Thus, the effect of global coupling is averaged out. Additionally, the applied forcing amplitudes are comparably high, making an influence of global coupling even more unlikely.

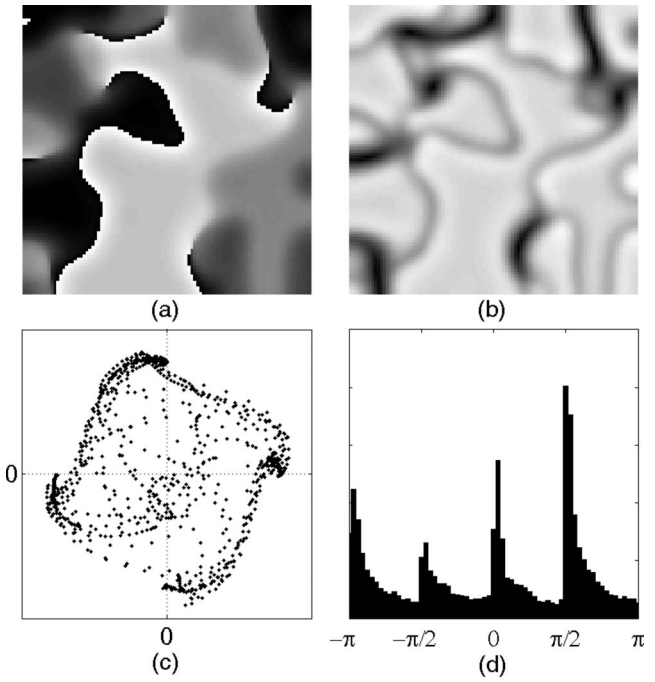

FIG. 7. Phase and amplitude representations of the cluster patterns shown in Fig. 6. (a) Phase pattern, (b) amplitude pattern, (c) phase portrait, and (d) phase histogram.

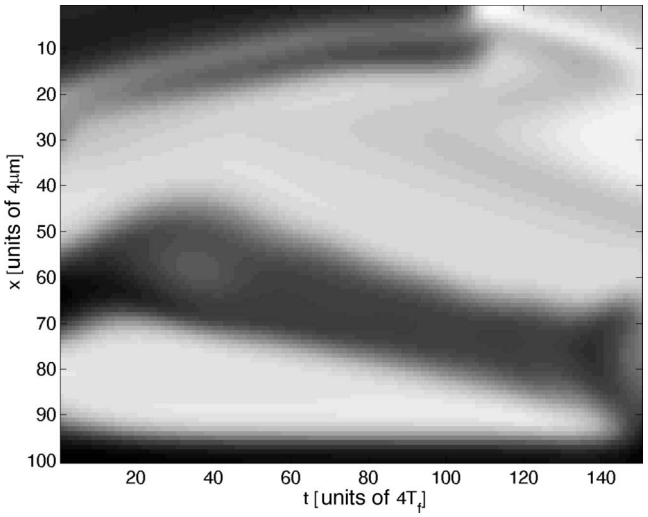

FIG. 8. Stroboscopic space-time plot showing the pattern evolution along a vertical line on the surface every fourth forcing cycle. For model parameters, see Fig. 6.

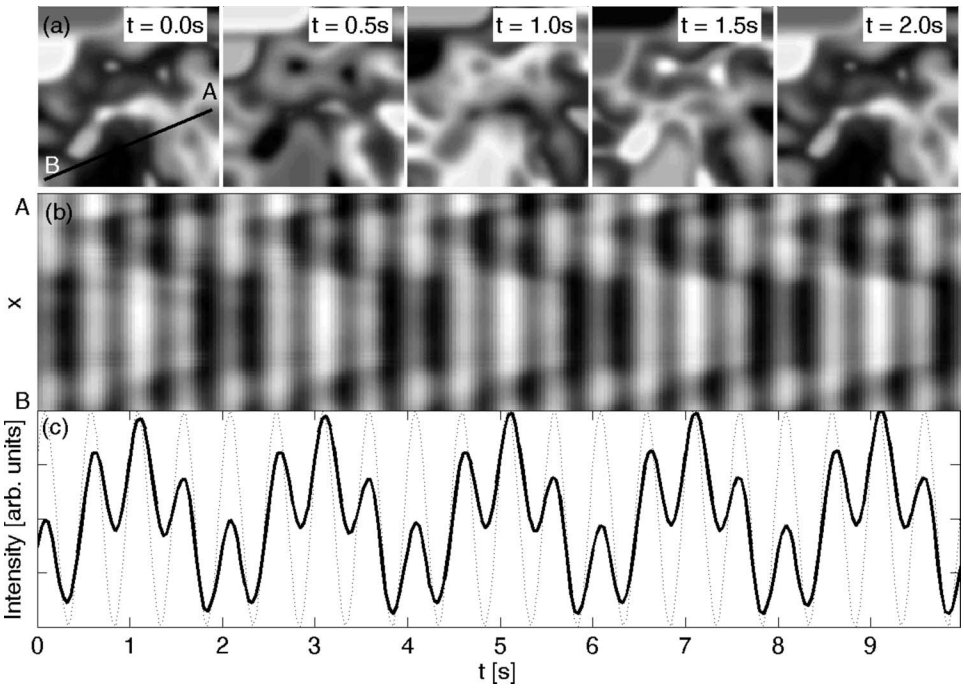

FIG. 9. Four-phase cluster and entrainment at 4:1 resonant forcing, KEE model. (a) Snapshots of CO coverage (size $400 \times 400\ \mu m^2$). (b) Space-time plot along the *AB* line (see top panel). (c) Local CO coverage at point *A* and forcing signal (dotted line). Model parameters: $\nu_f = 2$ Hz and $a = 0.086$.

An analysis of the KEE model reveals significant differences between the oscillation frequency of the single oscillator and the mean frequency on the surface, which appears to be higher in the turbulent state. While forcing with the fourth harmonic of the natural frequency of the single oscillator leads to 3:1 entrained three-phase patterns, 4:1 entrainment could be obtained by forcing with the fourth harmonic of the mean oscillation frequency. Weak detuning leads to the appearance of turbulent regions, similar to the experimental results. A main result is that the natural frequency of the single oscillator is not the characteristic frequency regarding entrainment and pattern formation. In contrast to the nonturbulent state, where the natural frequency of the single oscillator is identical with the oscillation frequency of the extended system, in the turbulent state the system oscillates at higher frequencies due to diffusive interaction of the surface elements. Interestingly, a similar frequency increase with respect to homogeneous oscillations was found for the spiral-wave oscillation frequency in the BZ reaction [18]. There, simulations showed entrainment when using the homogenous oscillation frequency and quasiperiodic behavior when forcing with the (higher) spiral-wave frequency, which is in contrast to our findings for the turbulent case. This is of major impact for the attempt of controlling the system by resonant forcing. Let us imagine a forcing with the fourth harmonic of the mean frequency of the turbulent system. In the moment where phase clusters appear, regions of surface elements are oscillating with the same phase and diffusion between these elements vanishes. Then we expect these elements to have similar properties as a single oscillator and, therefore, the same oscillation frequency. The surface elements within the clusters are then detuned and no longer in resonance with the forcing signal. On the other hand, during forcing with the fourth harmonic of the single oscillator's frequency, surface elements in the turbulent state and on the cluster boundaries are not in resonance. The detuning within the cluster boundaries might be the reason why even when using a regular four-phase pattern as the initial condition, we could not obtain stationary clusters. The situation differs strongly from resonant forcing of a reaction-diffusion system in a nonturbulent state. Numerical simulations of the KEE model in the nonturbulent regime reproduce traveling four-phase clusters as well as two-phase clusters at higher amplitude (not shown), as obtained before by different numerical models [14,19]. The greater the difference between these two

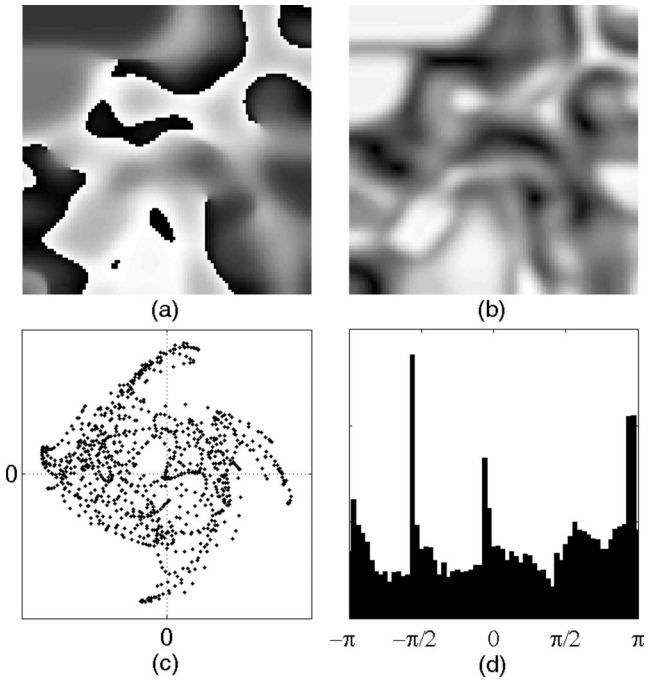

FIG. 10. Phase and amplitude representations of the cluster patterns given in Fig. 9. (a) Phase pattern, (b) amplitude pattern, (c) phase portrait, and (d) phase histogram.

characteristic frequencies, the more difficult it is to entrain both turbulent and phase-clustered regions. A necessary condition for entrainment of the phase clusters is that the forcing frequency lie within the respective Arnol'd tongue of the single oscillator. As the local oscillation frequency within the turbulent region varies (see Fig. 3), a comparable condition for entrainment of the surface elements with finite CO coverage gradients cannot be formulated. As the Arnol'd tongues are generally becoming smaller for higher harmonics, the effect of differing characteristic frequencies is becoming more and more pronounced by forcing the system with higher frequencies. While 2:1 forcing with the natural frequency of the single oscillator leads to 2:1 entrainment, 3:1 forcing resulted in bistability of 2:1 and 3:1 entrainment [17]. 4:1 forcing finally resulted in 3:1 entrainment, while 4:1 entrainment could not be obtained. Further investigation of high-frequency forcing of turbulent reaction-diffusion systems may give new insight into the nature of turbulence and may lead to new strategies for controlling chaos.

ACKNOWLEDGMENTS

Financial support from the Deutsche Forschungsgemeinschaft through Sonderforschungsbereich 555 "Complex Nonlinear Processes" and the Marie Curie European project "Patterns" is gratefully acknowledged.

[1] V. Petrov, Q. Ouyang, and H. L. Swinney, Nature (London) **388**, 655 (1997).
[2] V. K. Vanag, L. Yang, M. Dolnik, A. M. Zhabotinsky, and I. R. Epstein, Nature (London) **406**, 389 (2000).
[3] M. Kim, M. Bertram, M. Pollmann, A. von Oertzen, A. S. Mikhailov, H. H. Rotermund, and G. Ertl, Science **292**, 1357 (2001).
[4] M. Bertram, C. Beta, M. Pollmann, A. S. Mikhailov, H. H. Rotermund, and G. Ertl, Phys. Rev. E **67**, 036208 (2003).
[5] C. Beta, M. Bertram, A. S. Mikhailov, H. H. Rotermund, and G. Ertl, Phys. Rev. E **67**, 046224 (2003).
[6] J. Wolff, A. G. Papathanasiou, I. G. Kevrekidis, H. H. Rotermund, and G. Ertl, Science **294**, 134 (2001).
[7] M. Bertram, C. Beta, H. H. Rotermund, and G. Ertl, J. Phys. Chem. B **107**, 9610 (2003).
[8] V. K. Vanag, A. M. Zhabotinsky, and I. R. Epstein, Phys. Rev. Lett. **86**, 552 (2001).
[9] L. Glass, Nature (London) **410**, 277 (2001).
[10] M. Braune and H. Engel, Chem. Phys. Lett. **211**, 534 (1993).
[11] O. Steinbock, V. Zykov, and S. C. Müller, Nature (London) **366**, 322 (1993).
[12] V. Hakim and A. Karma, Phys. Rev. E **60**, 5073 (1999).
[13] H. K. Park, Phys. Rev. Lett. **86**, 1130 (2001).
[14] C. Elphick, A. Hagberg, and E. Meron, Phys. Rev. Lett. **80**, 5007 (1998).
[15] P. Coullet and K. Emilsson, Physica A **188**, 190 (1992).
[16] C. Hemming and R. Kapral, Physica D **168-169**, 10 (2002).
[17] J. Davidsen, A. Mikhailov, and R. Kapral, Phys. Rev. E **72**, 046214 (2005).
[18] A. L. Lin, A. Hagberg, A. Ardelea, M. Bertram, H. L. Swinney, and E. Meron, Phys. Rev. E **62**, 3790 (2000).
[19] A. L. Lin, A. Hagberg, E. Meron, and H. L. Swinney, Phys. Rev. E **69**, 066217 (2004).
[20] M. Eiswirth and G. Ertl, Phys. Rev. Lett. **60**, 1526 (1988).
[21] P. S. Bodega, P. Kaira, C. Beta, D. Krefting, D. Bauer, B. M. Schulz, C. Punckt, and H. H. Rotermund, New J. Phys. **9**, 61 (2007).
[22] T. Engel and G. Ertl, Adv. Catal. **28**, 1 (1979).
[23] H. H. Rotermund, S. Jakubith, A. von Oertzen, and G. Ertl, J. Chem. Phys. **91**, 4942 (1989).
[24] C. Beta, Ph.D. thesis, Freie Universität Berlin, 2004.
[25] H. H. Rotermund, W. Engel, M. Kordesch, and G. Ertl, Nature (London) **343**, 355 (1990).
[26] K. Krischer, M. Eiswirth, and G. Ertl, J. Chem. Phys. **96**, 9161 (1992).
[27] M. Falcke, H. Engel, and M. Neufeld, Phys. Rev. E **52**, 763 (1995).